Nano World Journal

https://doi.org/10.17756/nwj.2023-s5-079

Review Article

Open Access

Role of Copper Nanocluster for Anion Sensing

Priyanka Sharma, Mainak Ganguly* and Mamta Sahu

Department of Chemistry, Manipal University, Jaipur, Rajasthan, India

***Correspondence to:**
Mainak Ganguly
Department of Chemistry,
Manipal University,
Jaipur, Rajasthan, India.
E-mail: humansense2009@gmail.com

Received: October 20, 2023
Accepted: December 22, 2023
Published: December 28, 2023

Citation: Sharma P, Ganguly M, Sahu M. 2023. Role of Copper Nanocluster for Anion Sensing. *NanoWorld J* 9(S5): S487-S495.

Published by United Scientific Group

Abstract

Copper, group 11 coinage metal nanoparticles are widely used for environmental applications. Though the usage of copper is cost effective the rapid aerial oxidation is a challenge for practical applications. Copper nanocluster (CuNC) size (< 2 nm) is a hot field of research for its strong emissive property due to interbond transition. Choice and manipulation of capping agent for contributing stability to the CuNC. The alteration of fluorescence, as well as color in the presence of various anions in a selective and sensitive way, has helped to design chemo-sensor of anions. Along with recognition techniques of synthesized CuNCs, the toxicity of anions, characteristics of NCs, the fate of analytes, mechanism of sensing, analysis of natural water samples, and spot analysis have been discussed in this review article. Mostly fluorescence of NCs was quenched specifically with a particular anion. This review may open a new window in environmental nanoscience in relation to the capping of copper clusters and anions.

Keywords

Copper nanocluster, Sensing, Anion, Mechanism

Introduction

Clusters of various metals with diameters like the electron's Fermi wavelength (2 nm or less than 2 nm) exhibited strong molecule-like as well as dimeter-based visual and fluorescence characteristics, along with magnetic and chiral features [1-5]. When plasmonic particles interact with an electromagnetic field, the collective oscillations of conduction band electrons (typical of nanoparticles) no longer dominate in the ultra-tiny magnitude regime, which separates the energy band continuum into discrete energy levels [6-9]. Quantal or unique state optical absorption spectra exhibit several molecular-like properties [10, 11]. One of the few naturally occurring metals that may be used right away is copper [12]. Enzymes are created when copper reacts with specific proteins and serves as a catalyst for a variety of biological processes [13]. According to a study, copper deficiency was one factor raising the risk of coronary heart disease [14]. Additionally, Wilson's, Parkinson's, Alzheimer's disease, obesity, and diabetes were all caused by copper imbalances in humans [15]. Cu^{2+} can enter the body through polluted water, brought on consumer and industrial leftovers, or through acid rain-induced heavy metals in soil. Considering these effects, the United States Environmental Protection Agency (USEPA) designates copper as a possible trace contaminant and sets an allowed limit of 1.3 ppm (30 μM) of copper in intake-water. Human blood typically contains 15.7 ~ 23.6 μM of Cu^{2+}. Monitoring the amount of copper in intake water or other ecological fonts is crucial [16]. Luminescent CuNCs have emerged as an important class

of supplies for detection and catalysis due to their inimitable photo-physical possessions [17-20]. Unlike the formation of gold and silver NCs [21-25], the production of extremely tiny and highly stable CuNCs is still an infant [26-28], due to the intrinsic prone of the single-nanosized CuNCs to aggregate and oxidize in air [29]. Because of the great susceptibility to oxidation, atomically accurate CuNCs stability is a significant problem. The development of synthetic protocols, use of mild and inert conditions, choice of suitable ligands with distinctive structures and high metal binding affinities, purpose of various captivating structures or geometries, and the stability issue have been partially addressed over the past few decades.

CuNCs

The formation of gold and silver NCs has received a lot of attention in the research on noble metal NCs. In comparison to other precious metals, copper is comparatively abundant and inexpensive. CuNCs, on the other hand, are less stable because of their high oxidation susceptibility, and their luminescence quantum-yield (QY) is lower [30]. In recent years, efforts have been undertaken to improve the physicochemical and optical properties of CuNC to widen their applicability in a variety of domains, including sensing and nanodrugs [31, 32]. CuNC has a luminescence that is connected to inter-band transitions between occupied d-bands and the Fermi level [33]. The emission peaks red-shifted due to the quantum confinement effect when the cluster size rose in the order of Cu_5 < Cu_{13} < Cu_{20}. A similar effect was observed with CuNC of ultra-fine diameters (0.8 nm) [34, 35] (Figure 1).

Anions Detection via CuNC

Detection for nitrite

Common pollutants like nitrite (NO_2^-) ions can indicate organic contamination in freshwater and sewage by grouping with another form of N_2 [36, 37]. There are several detrimental health effects that could occur when NO_2^- ions in drinking water reach dangerously high levels, especially for infants and young children. Some illnesses, such as stomach or esophageal cancer, are suspected to be connected to NO_2^- ion intake [38-40]. The supreme adulteration limit of NO_2^- ions in intake-water was determined at 1 milligram N L^{-1} (71 µM) by the USEPA [41]. Many methods for detecting NO_2^- ions have been developed, including chromatography [42, 43], electrochemistry [44, 45], spectrophotometry [46-48], surface enhanced Raman-scattering [49], chemiluminescence [50, 51], or fluorometry [52-54].

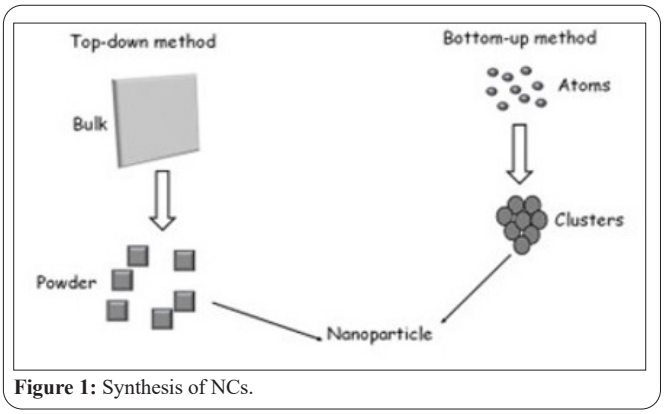

Figure 1: Synthesis of NCs.

In an aqueous solution, Zheng et al. [55] demonstrated an easy one step synthesis of high luminescence CuNC without the necessity for stabilizing agents, severe reductants, or organic medium. The luminescent CuNCs were selectively reduced by NO_2^- ions. The luminescence of the produced CuNC was robust and steady at 448 nm wavelength over a large pH range (6 - 8). NO_2^- ions were introduced to the CuNC solution, the degrees of slaking steadily decrease by rising pH 6 - 8. The addition of NO_2^- ions (500 µM) reduces the luminescence intensity of CuNC by about 90%. The linearity was generated in the ranges from 12.6 nM to 125.0 µM and 125.0 to 5000.0 µM. The limit of detection (LOD) for NO_2^- ions was estimated to be 3.60 nM (S/N = 3), which was significantly lesser than the EPA's supreme adulteration limit for NO_2^- ions in intake water (Figure 2).

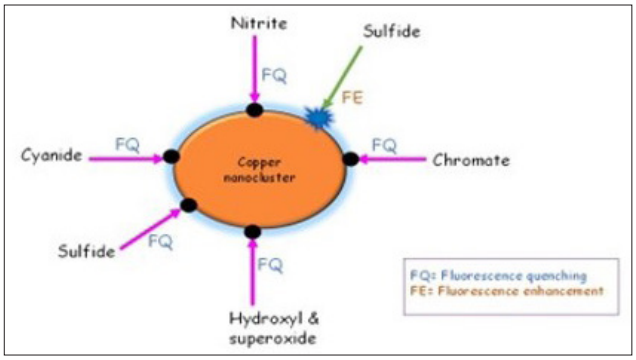

Figure 2: CuNC for anion sensing.

Real water analysis

Zheng et al. [55] showed the proposed sensor's potential utility by using it to sense NO_2^- ions in real-world samples. According to Han and Chen [56], the presence of CuNCs considerably improved the mild chemiluminescence that was produced when folic acid (FA) and diperiodatoargentate(III) (DPA) interacted in acid media. They found that NO_2^- ions inhibited the luminescence signal of the DPA-CuNCs-FA composite, and that intensity of the inhibited chemiluminescence was comparative to the NO_2^- ions in the range of 1.0 - 80.0 µM. DPA-CuNCs complex chemiluminescence intensity rose linearly with the FA content. The linear range was 0.1 to10 µM, the regression calculation was I = 387.9 (FA) (µM) + 191.0 (r = 0.998), and RSD was 1.37%. LOD was to be 69.9 nM. With increasing nitrite content, the chemiluminescence intensity of the DPA-CuNC-FA complex dropped linearly. The linear range nitrite determination was 1.0 - 80.0 µM, I = 1367 log (NO_2^-) (10) + 14419.7 (r = 0.993) of the regression equations. The RSD was 2.3%, and the LOD was 0.095 µM.

Real water and food sample analysis

Real sample analysis for NO_2^- ion detection is shown below as reported by Han and Chen [56] (Table 1).

Detection for dichromate

The USEPA classified dichromate ($Cr_2O_7^{2-}$) as an extremely harmful poisonous chemical as a heavy metal

Table 1: Real sample analysis for NO_2^- ion detection as reported by Han and Chen [56].

Sample	Added (µg/g)	Found (µg/g)	RSD (%)	Recovery (%)
Tap water	-	0.44 ± 0.010	2.3	-
	1.0	1.41 ± 0.020	1.4	97.0
	1.5	1.92 ± 0.0400	2.1	98.7
Spring water	-	0.13 ± 0.0050	3.8	-
	0.2	0.34 ± 0.013	3.8	105
	0.3	0.44 ± 0.018	4.1	103
Pickled vegetables	-	1.38 ± 0.0400	2.3	-
	2.0	3.37 ± 0.1100	3.3	99.5
	3.0	4.28 ± 0.170	4.0	96.7
Sausage	-	3.91 ± 0.160	4.1	-
	5	8.69 ± 0.310	3.4	95.6
	10	13.6 ± 0.580	4.4	96.9

pollutant [57]. When the (Cr(VI)) in water exceeds 0.10 mg/L, physiology (stomach, lungs, liver, and kidneys) is greatly affected via the excess limit of dichromate [58, 59].

Bai et al. [60] observed an easy and expedient phenomenon for detecting $Cr_2O_7^{2-}$ ions and Cd^{2+} ions using ratiometric and visual detection. They utilized glutathione as a starting ingredient to make cyan-emitting carbon dots (GSH@CDs). The correlation coefficient is 0.996, and the LOD was $Cr_2O_7^{2-}$ 0.9 µmol/L. The CDs@GSH-CuNCs solutions were incubated by varying ($Cr_2O_7^{2-}$) under daylight conditions. The CDs@GSH-CuNCs samples transformed from yellowish translucent to turbid under daytime illumination as $Cr_2O_7^{2-}$ concentrations increased, indicating that the CDs@GSH-CuNCs were increasingly damaged with $Cr_2O_7^{2-}$ ions. With increasing $Cr_2O_7^{2-}$ concentrations, the CDs@GSH-CuNCs solutions transformed from green-yellow to green luminescence under an ultraviolet lamp.

Khonkayan et al. [61] employed CuNCs, coated by 4,6-diamino-2-mercaptopyrimidine (CuNCs-DAMP), as a luminous probe to establish a two-step technique for *in situ* diffusive solid-state- phase-extraction of chromium ion. CrO_4^{2-} ion could diminish the excitation-intensity (through absorption) of CuNCs-DAMP, resulting in a drop in emission-intensity. CuNCs-DAMP had the maximum fluorescence intensity, while CrO_4^{2-} was not present. The lowermost luminesce intensity could be detected at the maximum (CrO_4^{2-}). With the existence of different anions, the luminescence spectra of CuNCs-DAMP did not alter considerably. The substantially reduced luminescence intensity could be detected exclusively in the occurrence of CrO_4^{2-} without any shift. Only CrO_4^{2-} could exhibit the inner filter upshot on the luminescence emission of CuNCs-DAMP except another anions (SO_3^-, COO^-, Cl^-, PO_4^{3-}, Br^-, SO_4^{2-}, CO_3^{2-}, NO_2^-, IO_3^-, ClO_4^-, I^-, BO_3^-, $B_2O_7^{4-}$, $P_2O_7^{4-}$, F^-, SCN^-, CN^-, $S_2O_8^{2-}$, IO_4^-, NO_3^-, and MnO_4^-). Within the array of 0.0 - 150.0 µM, a good linear connection between fluorescence intensity or CrO_4^{2-} attentiveness was obtained. F_0-F = 4.42 x (CrO_4^{2-}, mM) + 12.72 was the linear regression equation, with a correlation coefficient of 0.9896. The fluorescent probe's LOD and limit of quantification were 8.5 µM and 21.7 µM, respectively.

Real water analysis

Khonkayan et al. [61] presented a novel technique for detecting a trace level of CrO_4^{2-} by using a pre-concentration phase former to measure with a choosy fluorescence probe. A groundwater sample was obtained in Kalasin province using poly-ethylene bottles or castoff instantly in the absence of the use of a conservation agent.

Detection of hydroxyl and superoxide ion

The reactive species of oxygen (ROS) was a part of radical and nonradical oxygen containing compounds produced by aerobic-metabolism that play an important role in physiological processes [62-64]. Unfettered ROS stages cause oxidative stress, which has been connected to a diversity of diseases, including Alzheimer's and Parkinson's [65-67]. Because of their high reactivity and harmful consequences, O_2^- and OH have received significant attention among ROS [68].

Jindal et al. [69] demonstrated the development of a luminescence nano-probe based on CuNCs for the detection of OH or O_2^- ratiometrically. Using a carbodiimide-activated coupling technique, (-COOH) compounds of poly-methacrylic acid (PMAA) protected-copper nanocluster (P-CuNCs) were coupled by the ($-NH_2$) of BSA-protected-copper nanocluster (B-CuNCs) to generate a dual emitting fluorescent nano-probe (PCuNCs-BCuNCs). The luminescence peak at 445 nm rose constantly with the afterward reaction for incremental amounts of O^{2-}, whereas the peak at 652 nm remained nearly unaltered. The peak at 445 nm (P-CuNCs) was employed as the recognition element for determining O^{2-}, while the peak at 642 nm (B-CuNCs) was used as the reference signal. The unaffected emission at 652 nm could be attributed to B-CuNCs remaining stable in the presence of O^{2-}. P-CuNCs and B-CuNCs showed distinct fluorescence responses by exhibiting O^{2-} dependent quenching effects in the same concentration range. The dual-emission fluorescence intensity ratio (I_{445}/I_{652}) rose linearly with O^{2-} concentration (R^2 = 0.97), with corresponding LOD and limit of quantification of 1.8 µM and 6.1 µM, respectively. Under normal incubation conditions, the average emission ratio for P-CuNCs-B-CuNCs was determined to be 1.40 ± 0.09. The I_{green}/I_{red} ratio rose to 2.35 ± 0.34.

Detection of sulfide ion

The toxicity of sulfide (S^{2-}) was a big concern for the ecosystem. The S^{2-} ions perform an important role in the environment [70, 71]. S^{2-} can control cardiovascular system activity, blood pressure, immunological function. Nonetheless, sulfide was a major contributor to environmental contamination. Excess S^{2-} can cause Down-syndrome and Alzheimer's disease, as well as cirrhosis of the liver [72, 73].

Maruthupandia et al. [74] created a highly luminous CuNC in less than a minute. The CuNCs were effectively used as a luminescent probe to sense mercury and sulfide ions. Addition of 1.50 µM sulfide ion to CuNC-TG (1-Thio-β-D-glucose) caused a rise in comparative luminescence intensity from one to five minutes, after which it remained steady. Emission maxima of CuNCs-TG was observed at 430 nm.

The addition of 0.5 μM attentiveness of S^{2-} ions resulted in a decrease in CuNCs-TG fluorescence. The addition of S^{2-} at concentrations ranging from 1.0 to 5.5 μM likewise reduced the luminescence of CuNCs-TG to 430 nm. Under ultraviolet irradiation, the green color solution turned pale brown. The observed color and spectrum alterations were thought to be caused by the aggregation of CuNCs and the creation of the Cu-S composite. The detection limit was to be 1.020 nM. The linearity was detected to be good from 500 nM to 5.5 M. The QY of CuNCs-TG after varied concentrations of S^{2-} was discovered to be 6.6%.

Real water analysis

Real sample analysis for sulfide ion detection is shown below as reported by Maruthupandia et al. [74] (Table 2).

Wang et al. [75] used a one-pot procedure to generate 3-mercaptopropionic-acid functionalized CuNCs by aggregation-induced emission (AIE) triggered with copper (MPA@copper(II) CuNC) as a luminescent probe for the recognition of S^{2-} ions. The luminescence of other anions did not differ considerably from the MPA@Cu^{2+}CuNC. The luminescence of MPA@Cu^{2+}CuNC was significantly reduced with S^{2-} ions addition, changing from pinkish to dark brown. Under daylight conditions, the color of MPA@Cu^{2+}CuNC solution with S^{2-} ions added transformed from whitish to yellow brown, with essentially no-change in the existence of additional anions.

The effect of dissimilar anions co-existing with S^{2-} ions (pillars of green) on the sensor was observed. The consequence of dissimilar cations on the luminescence intensity of MPA@Cu^{2+}CuNC (pillars of red) and the effect on the sensor when dissimilar cations coexist with S^{2-} ions (green-pillars).

In the presence of S^{2-}, Zhang et al. [76] demonstrated a simple one-step green technique to produce natural silk fibroin (SF) coated CuNCs (CuNC@SF) with strong AIE capabilities. The fluorescence intensity of CuNC was modest. Addition of S^{2-} caused a substantial rise in the luminescence of CuNC@SF. When the attentiveness of S^{2-} ions was augmented to 100.0 μM, there was a three-fold increase in fluorescence emission intensity at 432 nm, with no discernible shift in emission wavelength. S^{2-} induction increased the QY of CuNC@SF from 1.6% - 4.9%. They observed a significant decrease in the absorption spectrum of CuNC@SF at 275 nm, indicating the contact of CuNCs with S^{2-} ions. The relationship between (F_0/F) for CuNCs and S^{2-} attentiveness was linear in the array of 5 μM - 110 μM, and a correlation coefficient of 0.99. LOD was 0.286 μM using a signal-to-noise ratio of three:one. Real sample analysis for sulfide ion detection is shown below as reported by Zhang et al. [76] (Table 3).

Jin et al. [77] demonstrated a unique way for using as produced yeast extract stabilized CuNC for sensitive and exclusive sulfide exposure. The fluorescence intensity of CuNC was greatly increased in the existence of both $Na_2S_2O_8$ and sulfide. CuNCs fluoresced strongly and consistently in phosphate buffer solution (pH 5.0). The luminescence intensity of the system was significantly enhanced after the addition of 0.5 mM $Na_2S_2O_8$ or 8 μM S^{2-} ions. The luminescence response of CuNC to S^{2-} ion at various pH levels. The luminescence of CuNC altered just slightly throughout the pH array of 3 - 11, as indicated. Though, after the accumulation of $Na_2S_2O_8$ and S^{2-} ions, the system's luminescence response revealed a substantial pH dependency. Although there was essentially little luminescence changed in the elementary condition (pH 8 - 11), there was a significant increase in fluorescence in the nonaligned and acidic solutions; pH 3 - 7. The proposed system's relative fluorescence intensity (F/F_0) exhibited a strong linear relationship versus S^{2-} ion concentration in the 0.02 - 0.8 μM range. LOD was determined to be 10.0 nM at S/N143, which was like or better than the detection limits got by other luminescent S^{2-} ion probes. Five consecutive measurements of 5 μM S^{2-} ions yielded an RSD of 4.30%.

Jin et al. [77] demonstrated the current approach for detecting S^{2-} ions in real world water samples, comprising tap water or hot spring-water. No noticeable S^{2-} ions were found in dilute tap water, while 0.143 ± 70.008 M S^{2-} ions were found in dilute hot spring-water. The recovery of water

Table 2: Real sample analysis for S^{2-} ion detection as reported by Maruthupandia et al. [74].

Tap water			River water		Pond water	
S^{2-} spiked (μM)	S^{2-} found (μM)	Recovery (%)	S^{2-} found (μM)	Recovery (%)	S^{2-} found (μM)	Recovery (%)
-	0	-	0	-	0	-
1	1.01	101 ± 0.2	0.998	99.8 ± 0.2	0.994	99.4 ± 0.2
2	1.98	99 ± 0.4	1.991	99.6 ± 0.3	198	99 ± 0.3

Table 3: Real sample analysis for S^{2-} ion detection as reported by Zhang et al. [76].

Sample	Detected (μM)	Added (μM)	Found (μM)	Recovery (%)	RSD* (%)
Tap water 1	**Not detected**	20	20.23	101.2	2.3
Tap water 2	**Not detected**	40	40.65	101.6	1.7
Tap water 1	**Not detected**	50	49.20	98.4	2.6
River water 1	**Not detected**	20	19.54	97.7	3.1
River water 2	**Not detected**	40	40.58	101.5	2.4
River water 3	**Not detected**	50	49.69	99.4	2.8

samples was also carried out, and results ranged from 93.4% to 100.8%. For three replicate measurements, RSD was less than 5%, indicating that the method was repeatable.

Yin et al. [78] suggested a ratiometric fluorescence approach for S^{2-} detection based on carbon-dots and self-assembled CuNC motivated by aluminum ions. Under single stimulation, SiCDs/CuNCs@Al^{3+} emitted both blue and red light. Interestingly, with repeated addition of S^{2-}, the red emission of the CuNC was consistently suppressed, but the blue luminescence emission of the carbon-dots was sustained. The linear range of the S^{2-} fluorescence spectrometer is 0.5 to 40 μM, with a LOD of 0.160 μM. The luminescence response of SiCDs/CuNC@Al^{3+} to S^{2-} ions demonstrates discrete, red- pink-blue change of color process, indicating that visual inspection was feasible. Without the use of a spectrometer, a transportable luminescence sensor was built employing the color-to-value alteration capability of a smart phone for precise visualization or measurable identification of S^{2-} ions. Luminescent test floorings were made using SiCDs/CuNCs@Al^{3+} to provide more convenient and rapid visual scrutiny of S^{2-} ions in the aqueous atmosphere. Based on the smartphone unified test floorings detector, the range of linearity of S^{2-} ions exposure was 1.0 - 40.0 μM, and the LOD was 0.420 μM.

Rashi et al. [79] demonstrated a luminescent probe, poly-allylamine hydrochloride (PAH) functionalized CuNC (CuNC@PAH), for the sensing of S^{2-} ions. The synthesis of the probe was based on the electro-static contact of negatively charged CuNC and the positively charged polymer, PAH. The extreme increment of the photoluminescence intensity of CuNC and the QY increment from 0.30 - 6.0% was observed. The steady state or time resolved luminescence experiments showed the aggregation-induced-emission phenomena as a mechanism for photoluminescence QY enhancement. The PAH @CuNCs exhibit high selectivity for aqueous S^{2-} ions. The probe exhibited a remarkable decrement of fluorescence responsible for S^{2-} ions with a LOD of 2.39 μM over an attentiveness array of 0.0 - 20.0 μM.

Detection of cyanide ions

Ding et al. [80] developed a simple method for fabricating a multifunctional chemosensing platform for the sensing of Hg(II), Co (III), and CN(I) in an aquatic solution using fluorescent CuNCs. They showed that salicylaldehyde could efficiently modify the luminescence and sensing properties of CuNC. CuNC showed a high intra-molecular charge-transfer emission at 500 nm in the presence of salicylaldehyde (SA), coupled with a reduction in the initial fluorescence intensity of CuNC at 430 nm. This luminescence on the state of SA-CuNC at 500 nm was discovered to be solely inhibited with cobalt and boosted by cyanide.

Cang et al. [81] showed a dual sensing probe based on analyte induced photoluminescence slaking of thio-salicylic acid (TA) coated CuNC aggregates for the detection of NO_2^- and cyanide (CN^-) ions. CN^- was detected using CuNC-TA aggregates in phosphate buffer (10.0 mM, pH 8). The graphs of $(I_{F0} - I_F)/I_{F0}$ and I_{F0}/I_F against NO_2^- and CN^- ion concentrations were linear over attentiveness arrays of 15.0 to 50.0 μM (R^2 = 0.96) and 0.010 to 1.0 μM (R^2 = 0.998), respectively.

Real water analysis

A lake water sample collected from the National Taiwan University campus was filtered using a syringe filter with a pore width of 0.22 μm. PB solutions (498.0 - 300.0 μl) containing CuNC-TA aggregates were added after aliquots (500 μl) of lake water were spiked with standard cyanide (1.0 - 100.0 μl) and nitrite (1.0 - 100.0 μl) solutions, with final concentrations of 10 mM for PB, 0.01 - 1.0 μM for cyanide, 15.0 - 50.0 μM for nitrite, and 0.025X for CuNC-TA aggregates.

Mechanism

Zheng et al. [55] showed that in an acidic solution, NO_2^- anions interacted with H^+ ions to generate nitrosyl cations (NO^+). Because NO_2^- anions and transitional NO^+ had larger standard reduction potentials than copper(II), the NO_2^- ions had a greater propensity to oxidize the CuNC, resulting in luminesce slaking. The following were some relevant equations:

$$2HNO_2 + 4H^+ + 4e^- \rightarrow N_2O + 3H_2O;\ E^0 = 1.29\ V \quad (1)$$

$$NO^+ + 4e^- \rightarrow NO;\ E^0 = 1.45\ V \quad (2)$$

$$Cu(II) + e^- \rightarrow Cu(0);\ E^0 = 0.33\ V \quad (3)$$

Han and Chen [56] demonstrated that the addition of CuNC to the DPA-FA complex increased luminescence intensity considerably but did not modify the situation of FA peaks, indicating that CuNC catalyzed the interaction between DPA and FA. Various high-energy cutoff filters were used to analyze the chemiluminescence spectra of those complex, including DPA-DA, DPA-CuNC-FA, and DPA-CuNC-FA-NO_2^-. In the presence of nitrite, the strength of the chemiluminescence and luminescence of the DPA-CuNC-FA complex was reduced. According to Zheng et al. [55] the CuNC could be reacted with NO_2^- to generate a non-luminescent ground state complex, resulting in luminescence slaking. The creation of pterin-6-carboxylic acid diminished when CuNC was consumed, causing the chemiluminescence signal to be repressed.

Jin et al. [77] showed that the presence of S^{2-} ion could cause the aggregation of dispersed CuNC in dilute solutions by creating Cu-S complex interactions to the surface of CuNC, hence increasing the luminescence of CuNC. CuNCs' fluorescence enhancement was attributed to the coupling actions with both $S_2O_8^{2-}$ and S^{2-}. CuNCs' surfaces became more sensitive to surrounding species, enhancing the interaction with S^{2-} in the solution, leading to CuNC aggregation. Finally, AIE effects resulted in considerable fluorescence enhancement of CuNCs.

According to Cang et al. [81], one potential explanation for NO_2^- induced large aggregate formation at pH 5 was its reduction-oxidation interaction with TA on the surfaces of CuNC, resulting in the damage of TA molecules from the surfaces of the CuNCs. In an acidic media, HNO_2 is known to be a potent oxidant ($2HNO_2 + 4H^+ + 4e^- \rightarrow 4N_2O + 3H_2O$;

E° = 1.29 V). After the addition of 20 mM NO_2^- ions, a peak at m/z 200.9 Dalton was found. The redox reaction of NO_2^- with TA resulted in the production of 2-sulfobenzoic acid. Sulfonic acid and thiol compounds exhibited a lower binding constant for copper. After adding 10.0 mM CN^- ions to CuNC-TA aggregates, the MS spectra revealed the development of copper$(CN)_2$-complexes (m/z = 114.93; theoretical calculation: 114.93).

Maruthupandia et al. [74] demonstrated that the positively diverged arc was observed owing to the existence of both dynamic and static slaking for S^{2-} ions. The slaking constant was determined to be 3.3 x 10^{-5} M^{-1}. CuS led to aggregation is one probable route for S^{2-} detection.

Wang et al. [75] described the optical characteristics of MPA@Cu^{2+} CuNC, as well as the potential AIE mechanism. The luminescent signals of the MPA@Cu^{2+} CuNC decreased as S^{2-} increased. S^{2-} was well known for its ability to create steady complex Cu_2S (Ksp = 2.6 x 10^{-48}) and CuS (Ksp = 6.30 x 10^{-36}) with Cu^+ and Cu^{2+} compounds, respectively. Due to copper's great affinity for the -SH group of MPA, which causes fluorescence, the direct interaction of Cu^+ with the thiol group was induced, but S^{2-} readily interacted with Cu^{2+} in aquatic solution to generate a steady Cu-S complex. The Cu^{2+} that first coordinated with the carboxylic group in MPA@Cu^{2+} CuNC would react with sulfide ion to generate a steady Cu-S complex, destroying the structure of the luminous group with direct quenching of the fluorescence of MPA@Cu^{2+} CuNC. S^{2-} served as an extinguishing agent in the preceding process, interacting with Cu^+ and Cu^{2+} to produce non-fluorescent stable molecules Cu_2S and CuS, resulting in static slaking of luminescence.

Fate

Zheng et al. [55] demonstrated that the Cu^0 $2p_{3/2}$ and $2p_{1/2}$ characteristics were responsible for the copper XPS peaks in CuNC at 932.1 and 952.0 eV, respectively. The lack of Cu^{2+} was supported by the absence of a copper $2p_{3/2}$ satellite peak at roughly 942 eV. The XPS peak for copper $2p_{3/2}$ shifted to higher binding energies of 934.8 and 954.7 eV in the existence of NO_2^- ions and with the appearance of a satellite peak at 944.2 eV.

Konkhayan et al. [61] employed TEM (transmission electron microscope) to examine the CuNC-DAMP's particle size. The CuNC-DAMP had adequate dispersity as evidenced by its narrow particle size distribution, lack of aggregation, and spherical shape with an average diameter of 3.3 ± 0.6 nm. The TEM image demonstrates that the CuNC-DAMP was NC-sized. With the addition of CrO_4^{2-} ion, the CuNC-DAMP retained almost its original size. This result demonstrated that there was no interaction or reaction between the DAMP-CuNCs and CrO_4^{2-}.

The CuNCs were ordered to form into massive nanoparticles of rod-like structure with an ~ thickness of 15 ± 2 nm and a dimension of 47 ± 2 nm with the addition of 100 µM S^{2-} ion, according to Zhang et al. [76] This was a much larger than CuNC, which had a size of 2.8 ± 0.5 nm.

According to Jin et al. [77], luminescent CuNC were well-discrete and typically sphere-shaped. According to TEM pictures, the size of CuNC was primarily spread in the narrow region of two to four nm. In contrast to free CuNCs, which only existed in the form of well-isolated single NCs, irregular aggregates of CuNCs were detected after the accumulation of S^{2-} ions. The aggregation of CuNCs was attributed to the S^{2-} ion-enhanced luminescence of the discrete CuNC. Microscopic images of Cu-NCs before and after the addition of S^{2-} ions clearly demonstrated the development of CuNC aggregates.

Cang et al. [81] demonstrated that the average size of as prepared CuNC-TA aggregates varied from 3.7 ± 0.5 nm (hundred counts) to up to 200 nm and 2.2 nm after the addition of NO_2^- ion (20 mM) and CN^- ions (10 mM), respectively.

Maruthupandia et al. [74] showed CuNC-TG particles were distributed, with an average particle size of 2.58 ± 0.03 nm determined by TEM micrograph and particle size histogram. The lattice spacing was to be 0.21 nm from the single CuNC. The TG-CuNCs produced were crystalline in form. CuNC-TG in the presence of 5.5 µM S^{2-} ion indicated the aggregated structure of nanoparticles. The aggregated particle dimension was determined to be 17 nm. The observed aggregation was ascribed to the production of the copper-sulfur complex. The energy dispersive X-ray spectra of CuNC-TG in the presence of 5.5 µM S^{2-} ion exhibited substantial S^{2-} signals at 2.3 KeV and Cu^{2+} signals at 8.09 KeV [82, 83].

Wang et al. [75] demonstrated that MPA@Cu^{2+} CuNC had an arbitrary dispersal state and a particle size distribution of 4 nm on average. The novel scattered MPA@Cu^{2+} CuNCs showed considerable aggregated clusters, when Cu^{2+} was added to cause the production of MPA@Cu^{2+} CuNC, and the particle size became bigger due to aggregation (average 22.4 nm). According to the scanning electron microscope pictures of CuNCs@MPA and MPA@Cu^{2+} CuNC, the accumulation of Cu^{2+} encouraged the aggregation of scattered CuNC-MPA to form MPA@Cu^{2+} CuNC. The presence of S^{2-} ions in the MPA@Cu^{2+} CuNC caused the aggregated Cu^{2+}@MPA-CuNCs to emerge as distinct states.

Spot Analysis

Zheng et al. [55] generated a paper-based cellulose acetate sensor for on-site visual exposure of NO_2^- ions. Because NO_2^- anions had a strong specific effect on CuNCs, depositing varying quantities of NO_2^- anions onto the paper-sensor resulted in clearly discernible color changes against the inventive background under ultraviolet-visible irradiation. Even NO_2^- ions as low as 25.0 µM could be detected with the paper sensor.

Conclusion

Fluorescent CuNC has been reviewed in the context of anion sensing. Though there are many reviews available for cation sensing, anion sensing is not available. The cost-effectiveness of copper has added and extra benefit for designing a sensing platform. Mainly fluorometry and rarely

colorimetry has been employed for sensing purposes. This review indicates the capping of NCs to contribute stability with prototype applications. Selectivity and sensitivity and mechanistic ground are the main parameters for designing a chemosensor. All such factors have been carefully illustrated in this review article. The future generation, interested in venture into the field of environmental nanoscience may be sufficiently benefit with this review. Moreover, for enhancing the fundamental knowledge of cluster chemistry this review will be hopefully highly beneficial.

Acknowledgements

None.

Conflict of Interest

There is no conflict of interest.

Funding

There is no funding to disclose.

References

1. Wood DM, Ashcroft NW. 1982. Quantum size effects in the optical properties of small metallic particles. *Phys Rev B* 25(10): 6255. https://doi.org/10.1103/PhysRevB.25.6255
2. Wang Z, Chen B, Rogach AL. 2017. Synthesis, optical properties and applications of light-emitting copper nanoclusters. *Nanoscale Horiz* 2(3): 135-146. https://doi.org/10.1039/c7nh00013h
3. Pavliuk MV, Gutiérrez AS, Hattori Y, Messing ME, Czapla-Masztafiak J, et al. 2019. Hydrated electron generation by excitation of copper localized surface plasmon resonance. *J Phys Chem Lett* 10(8): 1743-1749. https://doi.org/10.1021/acs.jpclett.9b00792
4. Ganguly M, Pal J, Das S, Mondal C, Pal A, et al. 2013. Green synthesis and reversible dispersion of a giant fluorescent cluster in solid and liquid phase. *Langmuir* 29(34): 10945-10958. https://doi.org/10.1021/la402440z
5. Ganguly M, Jana J, Pal A, Pal T. 2016. Synergism of gold and silver invites enhanced fluorescence for practical applications. *RSC Adv* 6(21): 17683-17703. https://doi.org/10.1039/c5ra26430h
6. Garrido LV, Gonçalves JM, Rocha JC, Bastos EL, Toma HE, et al. 2020. Intriguing plasmonic and fluorescence duality in copper nanoparticles. *Plasmonics* 15: 1213-1219. https://doi.org/10.1007/s11468-020-01143-5
7. Sahu M, Ganguly M, Doi A. 2023. Metal-enhanced fluorescence due to salicylaldehyde-silver nanoparticle interactions for Fe^{3+} sensing. *ChemistrySelect* 8(25): e202301017. https://doi.org/10.1002/slct.202301017
8. Ziashahabi A, Ghodselahi T. 2013. Localized surface plasmon resonance properties of copper nano-clusters: a theoretical study of size dependence. *J Phys Chem Solids* 2013. 74(7): 929-933. https://doi.org/10.1016/j.jpcs.2013.02.009
9. Lu Y, Wei W, Chen W. 2012. Copper nanoclusters: synthesis, characterization and properties. *Chin Sci Bull* 57: 41-47. https://doi.org/10.1007/s11434-011-4896-y
10. Li D, Chen Z, Mei X. 2017. Fluorescence enhancement for noble metal nanoclusters. *Adv Colloid Interface Sci* 250: 25-39. https://doi.org/10.1016/j.cis.2017.11.001
11. Lettieri M, Palladino P, Scarano S, Minunni M. 2022. Copper nanoclusters and their application for innovative fluorescent detection strategies: an overview. *Sens Actuators Rep* 4: 100108. https://doi.org/10.1016/j.snr.2022.100108
12. Sharma P, Ganguly M. 2023. Copper-enhanced fluorescence: a novel platform for the sensing of hydrogen peroxide. *New J Chem* 47(16): 7481-7485. https://doi.org/10.1039/d3nj00507k
13. Tapiero H, Townsend DÁ, Tew KD. 2003. Trace elements in human physiology and pathology. Copper. *Biomed Pharmacother* 57(9): 386-398. https://doi.org/10.1016/s0753-3322(03)00012-x
14. Chaudhary N, Gupta PK, Eremin S, Solanki PR. 2020. One-step green approach to synthesize highly fluorescent carbon quantum dots from banana juice for selective detection of copper ions. *J Environ Chem Eng* 8(3): 103720. https://doi.org/10.1016/j.jece.2020.103720
15. Sivaraman G, Iniya M, Anand T, Kotla NG, Sunnapu O, et al. 2018. Chemically diverse small molecule fluorescent chemosensors for copper ion. *Coord Chem Rev* 357: 50-104. https://doi.org/10.1016/j.ccr.2017.11.020
16. Liu S, Wang YM, Han J. 2017. Fluorescent chemosensors for copper(II) ion: structure, mechanism and application. *J Photochem Photobiol C Photochem Rev* 32: 78-103. https://doi.org/10.1016/j.jphotochemrev.2017.06.002
17. Rotaru A, Dutta S, Jentzsch E, Gothelf K, Mokhir A. 2010. Selective dsDNA-templated formation of copper nanoparticles in solution. *Angew Chem Int Ed* 49(33): 5665-5667. https://doi.org/10.1002/anie.200907256
18. Qing Z, He X, Qing T, Wang K, Shi H, et al. 2013. Poly(thymine)-templated fluorescent copper nanoparticles for ultrasensitive label-free nuclease assay and its inhibitors screening. *Anal Chem* 85(24): 12138-12143. https://doi.org/10.1021/ac403354c
19. Tam JM, Tam JO, Murthy A, Ingram DR, Ma LL, et al. 2010. Controlled assembly of biodegradable plasmonic nanoclusters for near-infrared imaging and therapeutic applications. *ACS Nano* 4(4): 2178-2184. https://doi.org/10.1021/nn9015746
20. Jia X, Yang X, Li J, Li D, Wang E. 2014. Stable Cu nanoclusters: from an aggregation-induced emission mechanism to biosensing and catalytic applications. *Chem Commun* 50(2): 237-239. https://doi.org/10.1039/c3cc47771a
21. Xie J, Zheng Y, Ying JY 2009. Protein-directed synthesis of highly fluorescent gold nanoclusters. *J Am Chem Soc* 131(3): 888-889. https://doi.org/10.1021/ja806804u
22. Guo W, Yuan J, Dong Q, Wang E. 2010. Highly sequence-dependent formation of fluorescent silver nanoclusters in hybridized DNA duplexes for single nucleotide mutation identification. *J Am Chem Soc* 132(3): 932-934. https://doi.org/10.1021/ja907075s
23. Sun J, Jin Y. 2014. Fluorescent Au nanoclusters: recent progress and sensing applications. *J Mater Chem C* 2(38): 8000-8011. https://doi.org/10.1039/c4tc01489h
24. Zhang J, Chen C, Xu X, Wang X, Yang X. 2013. Use of fluorescent gold nanoclusters for the construction of a NAND logic gate for nitrite. *Chem Commun* 49(26): 2691-2693. https://doi.org/10.1039/c3cc38298b
25. Chen LY, Wang CW, Yuan Z, Chang HT. 2015. Fluorescent gold nanoclusters: recent advances in sensing and imaging. *Anal Chem* 87(1): 216-229. https://doi.org/10.1021/ac503636j
26. Wei W, Lu Y, Chen W, Chen S. 2011. One-pot synthesis, photoluminescence, and electrocatalytic properties of subnanometer-sized copper clusters. *J Am Chem Soc* 133(7): 2060-2063. https://doi.org/10.1021/ja109303z
27. Vilar-Vidal N, Blanco MC, López-Quintela MA, Rivas J, Serra C. 2010. Electrochemical synthesis of very stable photoluminescent copper clusters. *J Phys Chem C* 114(38): 15924-15930. https://doi.org/10.1021/jp911380s
28. Brege JJ, Hamilton CE, Crouse CA, Barron AR. 2009. Ultrasmall copper nanoparticles from a hydrophobically immobilized surfactant template. *Nano Lett* 9(6): 2239-2242. https://doi.org/10.1021/nl900080f

29. Anzlovar A, Orel ZC, Zigon, M. 2007. Copper(I) oxide and metallic copper particles formed in 1,2-propane diol. *J Eur Ceram Soc* 27(2-3): 987-991. https://doi.org/10.1016/j.jeurceramsoc.2006.04.131
30. An Y, Ren Y, Bick M, Dudek A, Waworuntu EHW, et al. 2020. Highly fluorescent copper nanoclusters for sensing and bioimaging. *Biosense Bioelectron* 154: 112078. https://doi.org/10.1016/j.bios.2020.112078
31. Hu X, Liu T, Zhuang Y, Wang W, Li Y, et al. 2016. Recent advances in the analytical applications of copper nanoclusters. *TrAC Trend Anal Chem* 77: 66-75. https://doi.org/10.1016/j.trac.2015.12.013
32. Qing T, Zhang K, Qing Z, Wang X, Long C, et al. 2019. Recent progress in copper nanocluster-based fluorescent probing: a review. *Microchim Acta* 186: 670. https://doi.org/10.1007/s00604-019-3747-4
33. Shahsavari S, Hadian S, Ghazvini, Saboor FH, Oskouie IM, et al. 2019. Ligand functionalized copper nanoclusters for versatile applications in catalysis, sensing, bioimaging, and optoelectronics. *Mater Chem Front* 3(11): 2326-2356. https://doi.org/10.1039/c9qm00492k
34. Vázquez-Vázquez C, Bañobre-López M, Mitra A, López-Quintela MA, Rivas J. 2009. Synthesis of small atomic Cu clusters in microemulsions. *Langmuir* 25(14): 8208-8216. https://doi.org/10.1021/la900100w
35. Shin DY, Won JS, Kwon JA, Kim MS, Lim DH. 2017. First-principles study of copper nanoclusters for enhanced electrochemical CO_2 reduction to CH_4. *Comput Theor Chem* 1120: 84-90. https://doi.org/10.1016/j.comptc.2017.10.001
36. Sreekumar N, Narayana B, Hegde P, Manjunatha B, Sarojini B. 2003. Determination of nitrite by simple diazotization method. *Microchem J* 74(1): 27-32. https://doi.org/10.1016/S0026-265X(02)00093-0
37. Gabbay J, Almog Y, Davidson M, Donagi A. 1977. Rapid spectrophotometric micro-determination of nitrites in water. *Analyst* 102(1214): 371-376. https://doi.org/10.1039/an9770200371
38. Zurcher DM, Adhia YJ, Romero JD, McNeil AJ. 2014. Modifying a known gelator scaffold for nitrite detection. *Chem Commun* 50(58): 7813-7816. https://doi.org/10.1039/c4cc02504k
39. Manassaram DM, Backer LC, Moll DM. 2006. A review of nitrates in drinking water: maternal exposure and adverse reproductive and developmental outcomes. *Environ Health Perspect* 114(3): 320-327. https://doi.org/10.1289/ehp.8407
40. Reed PI, Haines K, Smith PLR, House FR, Walters CL. 1981. Gastric-juice n-nitrosamines in health and gastroduodenal disease. *Lancet* 318(8246): 550-552. https://doi.org/10.1016/s0140-6736(81)90939-9
41. Jayawardane BM, Wei S, McKelvie ID, Kolev SD. 2014. Microfluidic paper-based analytical device for the determination of nitrite and nitrate. *Anal Chem* 86(15): 7274-7279. https://doi.org/10.1021/ac5013249
42. Doyle JM, Miller ML, McCord BR, McCollam DA, Mushrush GW. 2000. A multicomponent mobile phase for ion chromatography applied to the separation of anions from the residue of low explosives. *Anal Chem* 72(10): 2302-2307. https://doi.org/10.1021/ac991346z
43. Liu Z, Xi X, Dong S, Wang E. 1997. Liquid chromatography-amperometric detection of nitrite using a polypyrrole modified glassy carbon electrode doped with tungstodiphosphate anion. *Anal Chim Acta* 345(1-3): 147-153. https://doi.org/10.1016/S0003-2670(96)00631-9
44. Ning W, Xia C, Xiaolan C, Xanjun X, Lin G. 2010. Porous cuprite films: facile solution deposition and their application for nitrite sensing. *Analyst* 135(8): 2106-2110. https://doi.org/10.1039/c000086h
45. Tian Y, Wang J, Wang Z, Wang S. 2004. Electroreduction of nitrite at an electrode modified with polypyrrole nanowires. *Synth Met* 143(3): 309-313. https://doi.org/10.1016/j.synthmet.2003.12.014
46. Daniel WL, Han MS, Lee JS, Mirkin CA. 2009. Colorimetric nitrite and nitrate detection with gold nanoparticle probes and kinetic end points. *J Am Chem Soc* 131(18): 6362-6363. https://doi.org/10.1021/ja901609k
47. Afkhami A, Bahram M, Gholami S, Zand Z. 2005. Micell-mediated extraction for the spectrophotometric determination of nitrite in water and biological samples based on its reaction with p-nitroaniline in the presence of diphenylamine. *Anal Biochem* 336(2): 295-299. https://doi.org/10.1016/j.ab.2004.10.026
48. Kumar VV, Anthony SP. 2014. Highly selective silver nanoparticles-based label free colorimetric sensor for nitrite anions. *Anal Chim Acta* 842: 57-62. https://doi.org/10.1016/j.aca.2014.06.028
49. Liu X, Tang L, Niessner R, Ying Y, Haisch C. 2014. Nitrite-triggered surface plasmon-assisted catalytic conversion of p-aminothiophenol to p,p-dimercaptoazobenzene on gold nanoparticle: surface-enhanced Raman scattering investigation and potential for nitrite detection. *Anal Chem* 87(1): 499-506. https://doi.org/10.1021/ac5039576
50. Lin Z, Xue W, Chen H, Lin JM. 2011. Peroxynitrous-acid-induced chemiluminescence of fluorescent carbon dots for nitrite sensing. *Anal Chem* 83(21): 8245-8251. https://doi.org/10.1021/ac202039h
51. Li J, Li Q, Lu C, Zhao L. 2011. Determination of nitrite in tap waters based on fluorosurfactant-capped gold nanoparticles-enhanced chemiluminescence from carbonate and peroxynitrous acid. *Analyst* 136(11): 2379-2384. https://doi.org/10.1039/c0an00918k
52. Chen WY, Huang CC, Chen LY, Chang HT. 2014. Self-assembly of hybridized ligands on gold nanodots: tunable photoluminescence and sensing of nitrite. *Nanoscale* 6(19): 11078-11083. https://doi.org/10.1039/c4nr02817a
53. Liu H, Yang G, Abdel-Halim ES, Zhu JJ. 2013. Highly selective and ultrasensitive detection of nitrite based on fluorescent gold nanoclusters. *Talanta* 104: 135-139. https://doi.org/10.1016/j.talanta.2012.11.020
54. Yue Q, Sun L, Shen T, Gu X, Zhang S, et al. 2013. Synthesis of fluorescent gold nanoclusters directed by bovine serum albumin and application for nitrite detection. *J Fluoresc* 23: 1313-1318. https://doi.org/10.1007/s10895-013-1265-z
55. Zheng XJ, Liang RP, Li ZJ, Zhang L, Qiu JD. 2016. One-step, stabilizer-free and green synthesis of Cu nanoclusters as fluorescent probes for sensitive and selective detection of nitrite ions. *Sens Actuators B Chem* 230: 314-319. https://doi.org/10.1016/j.snb.2016.02.063
56. Han S, Chen X. 2019. Copper nanoclusters-enhanced chemiluminescence for folic acid and nitrite detection. *Spectrochim Acta A Mol Biomol Spectrosc* 210: 315-320. https://doi.org/10.1016/j.saa.2018.11.051
57. Lu BB, Jiang W, Yang J, Liu YY, Ma JF. 2017. Resorcin[4]arene-based microporous metal-organic framework as an efficient catalyst for CO_2 cycloaddition with epoxides and highly selective luminescent sensing of $Cr_2O_7^{2-}$. *ACS Appl Mater Inter* 9(45): 39441-39449. https://doi.org/10.1021/acsami.7b14179
58. He T, Zhang YZ, Kong XJ, Yu JM, Lv XL, et al. 2018. Zr(IV)-based metal-organic framework with T-shaped ligand: unique structure, high stability, selective detection, and rapid adsorption of $Cr_2O_7^{2-}$ in water. *ACS Appl Mater Interfaces* 10(19): 16650-16659. https://doi.org/10.1021/acsami.8b03987
59. Rakhunde R, Deshpande L, Juneja HD. 2012. Chemical speciation of chromium in water: a review. *Crit Rev Environ Sci Technol* 42(7): 776-810. https://doi.org/10.1080/10643389.2010.534029
60. Bai H, Tu Z, Liu Y, Tai Q, Guo Z, et al. 2020. Dual-emission carbon dots-stabilized copper nanoclusters for ratiometric and visual detection of $Cr_2O_7^{2-}$ ions and Cd^{2+} ions. *J Hazard Mater* 386: 121654. https://doi.org/10.1016/j.jhazmat.2019.121654
61. Khonkayan K, Sansuk S, Srijaranai S, Tuntulani T, Saiyasombat C, et al. 2017. New approach for detection of chromate ion by preconcentration with mixed metal hydroxide coupled with fluorescence sensing of copper nanoclusters. *Microchim Acta* 184: 2965-2974. https://doi.org/10.1007/s00604-017-2320-2
62. Lim NY, Ahn J, Won M, Choi W, Kim JS, et al. 2019. Novel cyanostilbene-based fluorescent chemoprobe for hydroxyl radicals and its two-photon bioimaging in living cells. *ACS Appl Bio Mater* 2(2): 936-942. https://doi.org/10.1021/acsabm.8b00796

63. Hai X, Guo Z, Lin X, Chen X, Wang J. 2018. Fluorescent TPA@ GQDs probe for sensitive assay and quantitative imaging of hydroxyl radicals in living cells. *ACS Appl Mater Interfaces* 10(6): 5853-5861. https://doi.org/10.1021/acsami.7b16094

64. Goetz ME, Luch A. 2008. Reactive species: a cell damaging rout assisting to chemical carcinogens. *Cancer Lett* 266(1): 73-83. https://doi.org/10.1016/j.canlet.2008.02.035

65. Rose S, Melnyk S, Pavliv O, Bai S, Nick TG, et al. 2012. Evidence of oxidative damage and inflammation associated with low glutathione redox status in the autism brain. *Transl Psychiatry* 2(7): e134. https://doi.org/10.1038/tp.2012.61

66. Cairns RA, Harris IS, Mak TW. 2011. Regulation of cancer cell metabolism. *Nat Rev Cancer* 11(2): 85-95. https://doi.org/10.1038/nrc2981

67. Ju E, Liu Z, Du Y, Tao Y, Ren J, et al. 2014. Heterogeneous assembled nanocomplexes for ratiometric detection of highly reactive oxygen species *in vitro* and *in vivo*. *ACS Nano* 8(6): 6014- 6023. https://doi.org/10.1021/nn501135m

68. Zhuang M, Ding C, Zhu A, Tian Y. 2014. Ratiometric fluorescence probe for monitoring hydroxyl radical in live cells based on gold nanoclusters. *Anal Chem* 86(3): 1829-1836. https://doi.org/10.1021/ac403810g

69. Jindal G, Garg S, Matai I, Packirisamy G, Sachdev A. 2021. Dual-emission copper nanoclusters-based ratiometric fluorescent probe for intracellular detection of hydroxyl and superoxide anion species. *Microchim Acta* 188: 13. https://doi.org/10.1007/s00604-020-04683-z

70. Yuan Z, Peng M, Shi L, Du Y, Cai N, et al. 2013. Disassembly mediated fluorescence recovery of gold nanodots for selective sulfide sensing. *Nanoscale* 5(11): 4683-4686. https://doi.org/10.1039/c2nr33202g

71. Vasimalai N, Fernández-Argüelles MT, Espiña B. 2018. Detection of sulfide using mercapto tetrazine protected fluorescent gold nanodots: the preparation of paper based testing kit for on-site monitoring. *ACS Appl Mater Interfaces* 10(2): 1634-1645. https://doi.org/10.1021/acsami.7b11769

72. Kang JH, Yang M, Yun D, Kim M, Lee H, et al. 2019. A dual-response sensor based on NBD for the highly selective determination of sulfide in living cells and zebrafish. *New J Chem* 43(10): 4029-4035. https://doi.org/10.1039/c8nj06352d

73. Liang M, Chen Y, Zhang H, Niu X, Xu L, et al. 2015. Fluorescence resonance energy transfer-based ratiometric fluorescent assay for highly sensitive and selective determination of sulfide anion. *Analyst* 140(19): 6711-6719. https://doi.org/10.1039/c5an01378j

74. Maruthupandia M, Thiruppathib D, Vasimalai N. 2020. One minute synthesis of green fluorescent copper nanocluster: the preparation of smartphone aided paper-based kit for on-site monitoring of nanomolar level mercury and sulfide ions in environmental samples. *J Hazard Mater* 392: 122294. https://doi.org/10.1016/j.jhazmat.2020.122294

75. Wang D, Wang Z, Wang X, Zhuang X, Tian C, et al. 2020. Functionalized copper nanoclusters-based fluorescent probe with aggregation-induced emission property for selective detection of sulfide ions in food additives. *J Agric Food Chem* 68(40): 11301-11308. https://doi.org/10.1021/acs.jafc.0c04275

76. Zhang G, Wang R, Shi L, Zhang C, Zhang Y, et al. 2019. Aggregation/assembly induced emission based on silk fibroin-templated fluorescent copper nanoclusters for "turn-on" detection of S^{2-}. *Sens Actuators B Chem* 279: 361-368. https://doi.org/10.1016/j.snb.2018.09.100

77. Jin L, Zhang Z, Tang A, Li C, Shen Y. 2016. Synthesis of yeast extract-stabilized Cu nanoclusters for sensitive fluorescent detection of sulfide ions in water. *Biosens Bioelectron* 79: 108-113. https://doi.org/10.1016/j.bios.2015.12.001

78. Yin C, Liu T, Wu M, Liu H, Sun Q, et al. 2022. Smartphone-integrated dual-emission fluorescence sensing platform based on carbon dots and aluminum ions-triggered aggregation-induced emission of copper nanoclusters for on-site visual detecting sulfur ions. *Anal Chim Acta* 1232: 340460. https://doi.org/10.1016/j.aca.2022.340460

79. Rashi, Bain D, Devi A, Chakraborty S, Patra A. 2023. Cationic polymer functionalized copper nanocluster-based fluorescent probe for the selective and sensitive detection of S^{2-} ions. *ACS Sustain Chem Eng* 11(5): 1995-2004. https://doi.org/10.1021/acssuschemeng.2c07388

80. Ding W, Chen Z, Cao W, Gu Y, Zhang T, et al. 2021. Copper nanoclusters with/without salicylaldehyde-modulation for multifunctional detection of mercury, cobalt, nitrite and cyanide ions in aqueous solution and bioimaging. *Nanotechnology* 32(14): 145704. https://doi.org/10.1088/1361-6528/abd4a2

81. Cang J, Wang CW, Chen PC, Lin YJ, Li YC, et al. 2017. Control of pH for separated quantitation of nitrite and cyanide ions using photoluminescent copper nanoclusters. *Anal Methods* 9(36): 5254-5259. https://doi.org/10.1039/c7ay01300k

82. Abdulla-Al-Mamun M, Kusumoto Y, Ahmmad B, Shariful Islam M. 2010. Photocatalytic cancer (HeLa) cell-killing enhanced with Cu–TiO_2 nanocomposite. *Top Catal* 53: 571-577. https://doi.org/10.1007/s11244-010-9489-5

83. Das G, Kakati N, Lee SH, Karak N, Yoon YS. 2014. Water soluble sodium sulfate nanorods as a versatile template for the designing of copper sulfide nanotubes. *J Nanosci Nanotechnol* 14(6): 4455-4461. https://doi.org/10.1166/jnn.2014.8282